Research Square

Preprints are preliminary reports that have not undergone peer review.
They should not be considered conclusive, used to inform clinical practice,
or referenced by the media as validated information.

Optimizing the Bell Crank Structure for Weight Reduction and Stiffness Enhancement in Formula Student Vehicles

Khairun Nasrin Rimi

khairun.nasrin@mte.wub.edu.bd

World University of Bangladesh

Md Saifur Rahman

Chittagong University of Engineering and Technology

Md Araful Haque

Ahsanullah University of Science and Technology

Nurul Islam Kajol

Masters in Business Administration, Harbin Institute of Technology

Zannatul Ferdous

Ahsanullah University of Science and Technology

Research Article

Keywords: Topology Optimization, Formula SAE (FSAE), Finite Element Analysis (FEA)

Posted Date: May 25th, 2026

DOI: https://doi.org/10.21203/rs.3.rs-9532970/v1

License: This work is licensed under a Creative Commons Attribution 4.0 International License.
Read Full License

Additional Declarations: No competing interests reported.

Optimizing the Bell Crank Structure for Weight Reduction and Stiffness Enhancement in Formula Student Vehicles

Khairun Nasrin Rimi[1*], Md Saifur Rahman[2], Md Araful Haque[3], Nurul Islam Kajol[4], Zannatul Ferdous[5]

[1]Department of Mechatronics Engineering, World University of Bangladesh, Dhaka, Bangladesh

[2]Department of Mechanical Engineering, Chittagong University of Engineering and Technology, Chattogram, Bangladesh

[\3]Department of Mechanical and Production Engineering, Ahsanullah University of Science and Technology, Dhaka, Bangladesh

[4]Masters in Business Administration, Harbin Institute of Technology, Shenzhen, China

[5]Department of Mechanical and Production Engineering, Ahsanullah University of Science and Technology, Dhaka, Bangladesh

Corresponding author

Email: khairun.nasrin@mte.wub.edu.bd

ORCID ID: https://orcid.org/0009-0002-7675-4880

Abstract— Formula SAE (FSAE) vehicles require lightweight, high-performance Bell cranks to optimize force transfer and suspension dynamics. This study addresses the challenges of reducing weight while ensuring structural integrity through advanced topology optimization techniques. Finite element analysis (FEA) in ANSYS was employed to redistribute material systematically, focusing on stress distribution to identify and eliminate low-stress zones while maintaining manufacturability. The study explored various materials, including AISI316L, AISI10Mg, Ti6Al4V, In718, Aluminum 6063, Aluminum 6061, Mild Steel, and Stainless Steel. Titanium alloy (Ti6Al4V) emerged as the top-performing material, offering a high safety factor of 15.0, 40% stress reduction, and minimal deformation but presenting challenges due to high cost and machining complexity. Inconel 718 also demonstrated strong performance but was similarly constrained by manufacturing difficulties. AISI316L proved to be a cost-effective alternative for moderately loaded components, increasing the safety factor from 8.43 to 14.28 and offering better machinability. Aluminium alloys (6061 and 6063) provided lightweight solutions but were limited by lower strength than steel and titanium alloys. The study achieved a 25–30% weight reduction in the optimized Bell crank, improving material efficiency and reducing fuel consumption in FSAE

vehicles. These findings offer valuable insights into material selection and structural optimization for high-performance automotive components.

Keywords: *Topology Optimization, Formula SAE (FSAE), Finite Element Analysis (FEA)*

Introduction

The objective of the global student engineering competition, Formula Student, is to develop and evaluate concepts for formula racing cars. Known also as Formula SAE (FSAE), this international collegiate competition is organized by the Society of Automotive Engineers (SAE), wherein university teams are tasked with designing, constructing, and racing a prototype Formula-style car [1]. The suspension system of an FSAE vehicle is crucial for its performance. Due to the constraints imposed by compact racetracks, such as vehicle dynamics, critical factors like track width and wheelbase significantly influence handling, weight transfer, and turning radius [2]. The SAE suspension must meet the following requirements: a) It must include shock absorbers. b) Suspension travel should not be less than 25.4 mm (1 inch) for both jounce and rebound. c) It must possess appropriate vibration attenuation capabilities. d) It should ensure the vehicle exhibits good handling and stability performance [3, 4]. Race cars typically employ double wishbone suspension systems with pull-rod or pushrod configurations due to their design simplicity and lightweight components [2].

A pushrod transmits suspension loads to a chassis-mounted bell crank, which is calibrated to achieve a slightly progressive compression ratio between wheel and damper movement. This configuration enhances driver comfort, predictability, and stability during aggressive cornering [5]. A classic example of a bell crank is found in bicycle brakes, where a 90-degree rotation applies handlebar force to the brake block. In automotive suspensions, these levers, in conjunction with pushrods or pull rods, engage the spring-damper unit, thereby serving as a fundamental element of ride quality [6]. In Formula SAE (FSAE) vehicles, bell crank design is subject to weight constraints. Reducing vehicle mass improves the power-to-weight ratio, particularly when engine power is limited, thereby enhancing overall performance [7]. To optimize bell crank performance while maintaining structural integrity, engineers employ structural topology optimization to effectively reduce its weight [8, 9].

Topology optimization is a computational structural design method that has rapidly evolved over the past over the past few decades. It automatically generates optimized layouts to maximize performance under specific design constraints [10]. Topology optimization is an advanced structural design method that achieves optimal structure configuration through rational material distribution, satisfying specified load conditions, performance, and constraints [11]. Unlike sizing and shape optimization, topology optimization operates independently of the initial configuration and encompasses a larger design space, positioning it as a leading structural design technique for high-performance, lightweight, and multifunctional structures, widely used in aerospace, automotive, architecture, and other industries [12]. It serves as an important engineering tool for improving structural performance and weight economy by optimizing material distribution within spaces. According to Sigmund and Maute [11], it plays a role in producing high-performance designs with less material, resulting in cost-effective solutions. It not only improves structural integrity but also revolutionizes existing design paradigms in mechanical engineering, fostering novel solutions through iterative computational methods.

Topology optimization is a mathematical method that optimizes material layout within a given design space, for a given set of loads, boundary conditions, and constraints to maximize the performance such as minimal weight, and maximal stiffness of the system [13]. The objective of structural topology optimization is to satisfy constraint conditions such as stress and displacement by optimizing the allocation of material and quantity in the design domain, material layout, and node connection mode [14]. A scalar field representing relative density per element represents material dispersion in a design domain. A value of = 1 indicates solidity, while a value of = 0 indicates emptiness. Initially an integer-programming problem, it is relaxed during optimization to allow for intermediate densities. Regardless of density, each element is assumed to be isotropic and homogeneous. Power-law interpolation is used to connect material parameters such as Young's modulus to density. Despite its appearance, this relationship was eventually proven for certain penalty powers (for example, p 3 for v = 1/3). This enables a heterogeneous material distribution inside the element domain, resulting in the formation of a microstructure of solid base material and void to match expected qualities at intermediate densities. Even seemingly simple 'mono-scale' density techniques, but with poor microstructures, can be seen as multi-scale [15].

The optimization objectives include minimizing the total strain energy of the design domain and minimizing the total displacement of the fixed domain. The shape optimization procedure is used to furtherly enhance structural performance [16]. To avoid the parasitic effect, the inactive volume constraint, and the intermediate material distribution induced by the self-weight loads [16]. Improving the performances of the device and reducing the material consumption are often conflicting. To reduce this BOOP (bi-objective optimization problem) vector TO (topology optimization) is developed. Vector optimizer has also a bottleneck issue of high computational cost of FEA [17].

The study presents a design optimization process utilizing laser vibrometer testing, reverse engineering, and structural topology optimization applied to a sidecar suspension bell crank. This methodology successfully reduced the bell crank's weight by 3%, maximum strain by 4.3%, and maximum von Mises stress by 16.5%, while increasing stiffness and natural frequency [5]. The bell crank underwent computational iterations using topological optimization, resulting in a 7% mass reduction while preserving stiffness properties; concurrently, the yield stress decreased by 43% (381 MPa), demonstrating its potential for weight reduction without compromising structural integrity in engineering design [18]. Only a limited number of studies have examined the topology optimization of bell cranks. This method is applied by Fornace [19] to reduce a Formula SAE vehicle's rear bell crank mass by at least 10% while preserving its yield strength. In response to the growing trend of optimizing parts in the automobile industry, Divadkar and Dhatrak (2023) do topology optimization for a truck's bell crank lever. The study focuses on improving the performance of the lever in AISI A514 steel by addressing stiffness and mass parameters. Through static analysis via FEA, the optimized design shows a 22% mass decrease (from 3395.71 grams to 2641.02 grams) and a 40% stiffness increase (from 389.32N/mm to 644.988N/mm), which aligns with the study's objectives [20]. Chauhan, Sah, and Kaushal (2021) investigate rocker designs for a Push-rod driven double wishbone suspension, incorporating rising motion ratios to avoid dynamic changes such as camber with wheel travel. Using AISI 1018 material with safe factors of safety of 4.8 and 3.3, the study achieves considerable weight savings of 79.4% and 74% for front and rear bell cranks, respectively [21].

A light weight bell crank and brake pedal model is designed and the FEA analysis is used for obtaining the maximum and minimum value of displacement, % of yield, tension/compression,

shear stress and von mises stress on the optimized design. The results of the design reflect that the weight of the bell crank has been reduced to 140 grams which is about 24% less weight than the existing design and the optimized weight of the brake pedal is reduced from 363g to 211g [22]. The bell crank weight is reduced by 59% and the brake pedal weight is reduced by 42%, while maintaining similar or better strength and stiffness characteristics [22]. A. M. Sharma et al crank is used in student formula prototypes which was subjected to a Pullrod force of 1650N, a Damper force of 24N and a Fulcrum force 1674N. Their initial design's stress and deformation was 143.09 MPa and 0.038mm while the final design had a stress generation of 491.65MPa and got deformed by 0.117mm. The material was also shifted from Aluminum 7075 T6 to Titanium 6Al-4V Grade 5 which resulted in weight reduction by 54% [20].

Chang and Lee (2008) demonstrated that integrating topology optimization during the conceptual stage can achieve superior structural efficiency, specifically realizing a 31% mass reduction in automotive brackets while simultaneously enhancing vibration durability and increasing natural frequency [23]. Lindan Yi used ANSYS software, takes the topology optimization design of automobile engine bracket, and makes the strength analysis, fatigue analysis, and model analysis of the new optimized bracket. The new bracket has less stress concentration and its fatigue analysis are not based on real road load spectrum [24]. In pursuit of a lighter brake pedal, Mohd Nizam embarked on a two-pronged approach: changing the material and employing topology optimization. This innovative strategy paid off handsomely, resulting in a remarkable 22% weight reduction compared to the existing model. By shedding unnecessary bulk while maintaining structural integrity, Nizam's optimized brake pedal not only boasts impressive efficiency but also paves the way for lighter, more fuel-efficient vehicles [25]. Zhang et al. performed Finite Element Analysis and topology optimization design for a new energy bus seat bracket using the variable density method [26]. The optimized bracket was lighter and showed improved mechanical properties.

Zhu, Zhang, & Xia (2016) survey topology optimization's recent advances in aircraft and aerospace design, discussing its applications in various structural layouts and its potential in dynamic responses, smart structures, and additive manufacturing [27]. Also, under fatigue life constraints, topology optimization of a subway air conditioning suspension support was performed using the SIMP method, leading to reductions in maximum displacement and stress by 80%, 93%, and 99%

under vertical, horizontal, and vertical loads, respectively, as studied by Xiao [28]. A study demonstrates a novel topology optimization method within a level set framework that addresses boundary uncertainty without the use of statistical information, allowing for precise control and enhanced structural resilience against stress concentration and crack initiation, resulting in improved robustness and lower computational costs [29].

The method used here can effectively generate lightweight substitute structures of great mechanical performance in many beam structures applications [13]. Topology optimization was applied to design patient-specific dental frameworks, resulting in a 16% reduction in maximum stress under a 50% volume fraction constraint, demonstrating improved structural integrity over traditional designs, as shown by Park's study [30]. A topology-optimized patient-specific mandibular reconstruction plate (TO-PSI) was biomechanically validated by Koper et al [31], with fractures occurring at a median peak load of 334 N (range: 304–336 N), falling within 30% of the predicted 378 N load, thereby confirming the effectiveness of the optimization approach.

This study systematically evaluates the structural feasibility of the FSAE bell crank by performing a comparative topology optimization across eight distinct material categories. While high-performance alloys like Ti 6414V and Inconel 718 are traditionally favored for their superior safety factors (up to 15.0) and significant stress reductions of approximately 40%, their high cost and machining complexity often limit practical implementation. Consequently, this research is undertaken to address the feasibility of utilizing more accessible materials, such as AISI 316L and Mild Steel, assessing their ability to maintain high structural rigidity and minimal deformation even after a targeted 50% mass reduction.

2. Numerical Modeling

2.1 CAD Modeling

For topological optimization, the bell crank of the formula car was chosen (Fig. 4). Dassault Solidworks was used for modelling purposes. The crank dimensions are shown here. Solidworks was chosen for its user-friendly modelling tools and easy export to ANSYS. Dimensions are finalized based on data and manufacturing restrictions. Three control arms feature eye-to-eye lengths of 86.14 mm, 78.26 mm, and 36 mm, with a hole diameter of 8 mm for mounting reasons. The mount has a thickness of 20 mm.

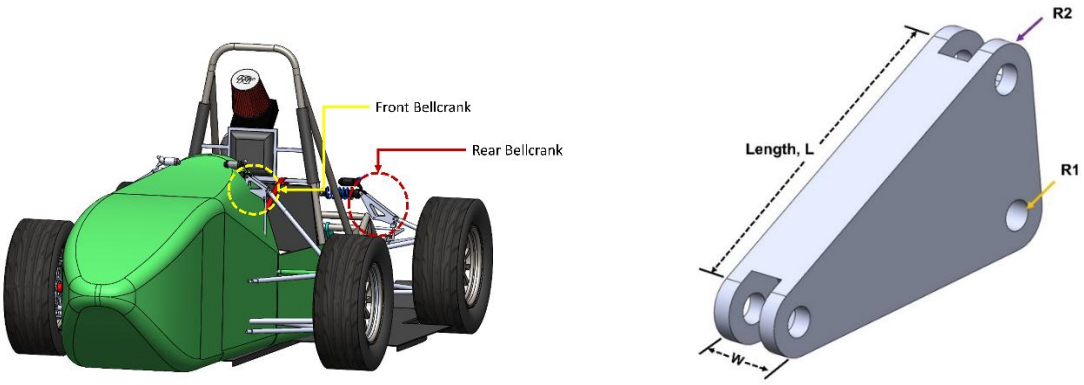


Figure-1: 3D model of the bell crank

2.2 Topology Optimization

Over the years, topology optimization has emerged as a dynamic area of research aimed at discovering innovative and unexpected designs across various disciplines, including solid mechanics, fluid dynamics, thermal dynamics, acoustics, and electromagnetism.

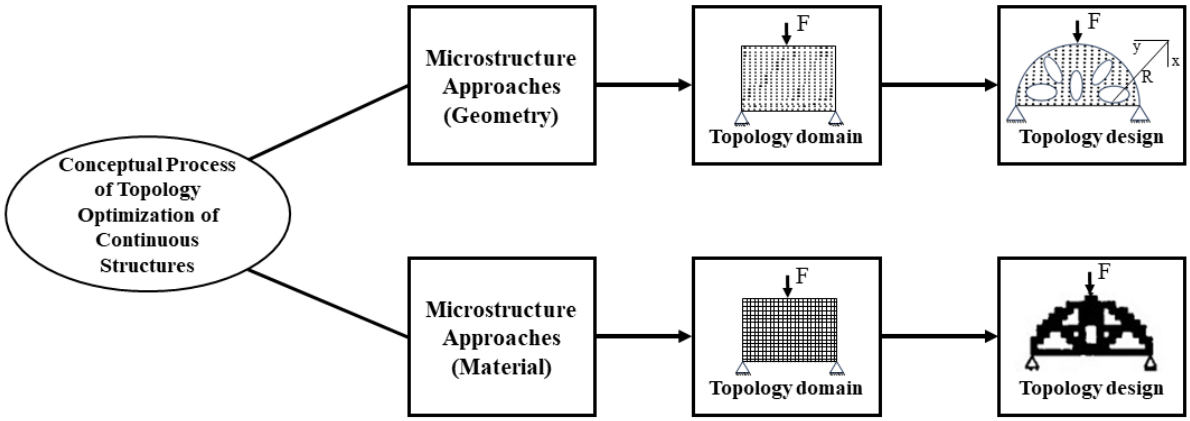


Figure-2: Conceptual Process of Topology Optimization of Continuous Structures

Topology optimization methods can be broadly divided into geometry-based and material-based techniques. Geometry-based methods optimize the layout and shape of microstructural elements within the design space, directly modifying the geometry to achieve the desired performance.

2.2.1 The SIMP Method

The SIMP (Solid Isotropic Material with Penalization) method is a popular technique for optimizing the topology of continuous structures. It uses a density parameter ρ (0 for void, 1 for solid) to interpolate material properties like stiffness, applying a penalization factor to promote solid-void distributions [32]. SIMP iteratively reallocates material to optimize goals such as stiffness and weight reduction while respecting constraints like volume fraction.

The SIMP approach employs elementwise density variables ρ_e as design variables to describe the topology layout. Therefore, the design domain Ω is discretized into cells or voxels, and each element e is assigned a density ρ_e. Although ρ_e, would ideally equal to 1 for material and 0 for the void, the design variable is here relaxed by allowing intermediate values $0 \leq \rho_e \leq 1$. Consequently, additional constraints (3-b-2) must be added to the original topology optimization problem subject to the volume constraint. Furthermore, the material interpolation of the constitutive tensor $\mathbb{C}_\rho$ is defined as

$$\mathbb{C}_\rho(\rho_e) = \mathbb{C}^- + \rho_e^p(\mathbb{C}^+ - \mathbb{C}^-), \rho_e \in [0,1] \quad (1)$$

where $\mathbb{C}^+$ and $\mathbb{C}^-$ correspond to the constitutive tensor of the stiff and soft materials, respectively. In addition, the parameter p stands for the penalization factor (typically $p \geq 3$). For a constant Poisson ratio, Eq. (1) can be written in terms of the Young's modulus E as

$$\mathbb{C}_\rho(\rho_e) = (E^- + \rho_e^p\ (E^+ - E^-))\mathbb{C}_{(1)}\ , \quad (2)$$

where E^+ and E^- represent the Young's modulus for the stiff and soft materials, respectively, and $\mathbb{C}_{(1)}$ correspond to the constitutive tensor with unit Young's modulus. Assuming that E^-can be defined as proportional to the high Young's modulus, E^+, via the contrast factor α, the resultant constitutive tensor $\mathbb{C}_\rho(\rho_e)$ is defined as $\mathbb{C}^+$ multiplied by a coefficient, which depends on the design variable of the element, i.e.,

$$\mathbb{C}_\rho(\rho_e) = (\alpha + \rho_e^p(1-\alpha))\mathbb{C}^+ \quad (3)$$

The global stiffness matrix $\mathbb{K}_\rho$ is obtained via the assembly of element stiffness matrices defined as

$$\mathbb{K}_e(\rho_e) = \int_{\Omega_e} \boldsymbol{B}^{\boldsymbol{T}}(\boldsymbol{x})\mathbb{C}_\rho(\boldsymbol{x})\boldsymbol{B}(\boldsymbol{x})\, d\Omega$$

$$= (\alpha + \rho_e^p(1-\alpha))\int_{\Omega_e} \boldsymbol{B}^{\boldsymbol{T}}(\boldsymbol{x})\mathbb{C}^{+}(\boldsymbol{x})\boldsymbol{B}(\boldsymbol{x})\, d\Omega \tag{4}$$

$$= (\alpha + \rho_e^p(1-\alpha))\mathbb{K}_e^{+}$$

with $\mathbb{K}_e^{+}$ being the element stiffness matrix considering stiff material for the element e.

Taking into account these two characteristics, the topology optimization problem becomes,

$$min \quad \mathcal{J}(\boldsymbol{u}(\boldsymbol{\rho}), \boldsymbol{\rho} \equiv \int_{\Omega} j(\boldsymbol{u}(\boldsymbol{\rho}), \boldsymbol{\rho}, \boldsymbol{x})\, d\Omega \qquad \text{(a)}$$

$\rho \in \mathcal{U}_{ad}$

subjected to:

$$\mathcal{C}_0(\boldsymbol{\rho}) \equiv \frac{|\Omega(\boldsymbol{\rho})|}{|\Omega|} - f \leq 0 \qquad \text{(b - 1),} \tag{5}$$

$$\mathcal{C}_e(\rho_e) \leq 0 \rightarrow 0 \leq \rho_e \leq 1,\ e : 1 \ldots N_e \qquad \text{(b - 2)}$$

governed by:

$$\mathbb{K}_{\boldsymbol{\rho}}\widehat{\boldsymbol{u}}_{\boldsymbol{\rho}}^{(\boldsymbol{i})} = \mathbf{f}^{(i)} \qquad \text{(c)}$$

where $|\Omega(\boldsymbol{\rho})|$ and $|\Omega|$ are respectively the stiff material volume and the design domain volume, and f is the prescribed volume fraction.

The sensitivity of the objective function (5-a), $\partial\mathcal{J}^{(I)}(\boldsymbol{u}(\boldsymbol{\rho}), \boldsymbol{\rho})/\,\partial_{\rho_e}$, is obtained via the adjoint technique so that the derivative of the unknown field $\boldsymbol{u}_{\rho}$ concerning the density ρ_e, $\partial\boldsymbol{u}(\boldsymbol{\rho})/\partial_{\rho_e}$, is not required to be computed. Additionally, the sensitivity of the volume constraint (5-b-1) concerning the density of the element e is equal to $|\Omega_e|/|\Omega|$. The sensitivity of the objective function for the three-topology optimization problems addressed in this work is given by

$$\frac{\partial\mathcal{J}^{(I)}(\boldsymbol{u}(\boldsymbol{\rho}),\boldsymbol{\rho})}{\partial_{\rho_e}} = -\omega_e(\rho_e)\widehat{\boldsymbol{u}}_{\boldsymbol{e}}(\boldsymbol{\rho})\mathbb{K}_e^{+}\widehat{\boldsymbol{u}}_{\boldsymbol{e}}(\boldsymbol{\rho}) \tag{6}$$

$$\frac{\partial\mathcal{J}^{(II)}(\boldsymbol{u}(\boldsymbol{\rho}),\boldsymbol{\rho})}{\partial_{\rho_e}} = -\omega_e(\rho_e)\sum_{\boldsymbol{i=1}}^{\boldsymbol{n_l}}\widehat{\boldsymbol{u}}_{\boldsymbol{e}}(\boldsymbol{\rho})\mathbb{K}_e^{+}\widehat{\boldsymbol{u}}_{\boldsymbol{e}}^{(\boldsymbol{i})}(\boldsymbol{\rho}) \tag{7}$$

$$\frac{\partial\mathcal{J}^{(III)}(\boldsymbol{u}(\boldsymbol{\rho}),\boldsymbol{\rho})}{\partial_{\rho_e}} = \omega_e(\rho_e)\widehat{\boldsymbol{u}}_{\boldsymbol{e}}^{(1)}(\boldsymbol{\rho})\mathbb{K}_e^{+}\widehat{\boldsymbol{u}}_{\boldsymbol{e}}^{(2)}(\boldsymbol{\rho}) \tag{8}$$

where $\omega_e(\rho_e) = p\rho_e^{p-1}(1-\alpha)$ and $\widehat{\boldsymbol{u}}_{\boldsymbol{e}}^{(\boldsymbol{i})}(\boldsymbol{\rho})$ represents the nodal displacement of the element e and state equation (i).

As mentioned in Section 1, a regulation technique must be applied to the original topology optimization problem to ensure the existence of a solution and avoid the formation of the so-called checkerboard patterns. Different filtering techniques modifying the element sensitivity are studied for the comparison, including a radial sensitivity filter computed using the convolution function and the filter based on the Helmholtz type differential equation. The solution to the filtering technique is denoted by $\widetilde{(\cdot)}$ and replaces the non-filtered sensitivity.

Considering the sensitivities of the objective function and volume constraint, the corresponding topology optimization problem can be solved by employing the Optimality Criteria (OC) method. The OC method seeks the fulfilment of the Karush-Kuhn-Tucker (KKT) conditions

$$\frac{\widetilde{\partial \mathcal{J}}}{\partial \rho_e} + \lambda \frac{\partial \mathcal{C}_0}{\partial \rho_e} = 0, e : 1 \dots N_e, \tag{9}$$

where λ is the Lagrange multiplier associated with the volume constraint $\mathcal{C}_0(\boldsymbol{\rho})$ such that the volume constraint is met and must be computed via a root-finding algorithm (e.g., a bisection method). Note that the element density ρ_e must be in the range of 0 to 1. The optimization conditions can be expressed as $B_e = 1$ here,

$$B_e = -\frac{\widetilde{\partial \mathcal{J}}}{\partial \rho_e}\left(\lambda \frac{\partial \mathcal{C}_0}{\partial \rho_e}\right)^{-1} \tag{10}$$

A heuristic updating scheme, proposed by Bendsoe and Kikuchi, is used to update the design variables and achieve convergence. For minimum mean compliance, the scheme is defined as

$$\rho_e^{(k+1)} = \begin{cases} \max\left(0, \rho_e^{(k)} - m\right) & \text{if } \rho_e^{(k)} B_e^{\eta} \le \max\left(0, \rho_e^{(k)} - m\right) \\ \min\left(1, \rho_e^{(k)} + m\right) & \text{if } \rho_e^{(k)} B_e^{\eta} \ge \min\left(1, \rho_e^{(k)} + m\right), \\ \rho_e^{(k)} B_e^{\eta} & \text{otherwise} \end{cases} \tag{11}$$

where m is the positive move limit, η is a numerical damping coefficient, and k represents the iteration counter. These two numerical parameters are typically set at 0.2 and 0.5 for minimum mean compliance. Eq. 10 is modified for compliant mechanism optimization problem to account for positive sensitivities as

$$B_e = max\left(\epsilon, -\frac{\widetilde{\partial J}}{\partial \rho_e}\right)\ \left(\lambda \frac{\partial C_0}{\partial \rho_e}\right)^{-1} \tag{12}$$

with ϵ being a small positive value. Equivalently, the updating scheme (11) can be expressed as

$$\rho_e^{(k+1)} = \begin{cases} \max\left(0, \rho_e^{(k)} - m\right) & \text{if } \rho_e^{(k)} B_e^{\eta} \le \max\left(\epsilon, \rho_e^{(k)} - m\right) \\ \min\left(1, \rho_e^{(k)} + m\right) & \text{if } \rho_e^{(k)} B_e^{\eta} \ge \min\left(1, \rho_e^{(k)} + m\right), \\ \rho_e^{(k)} B_e^{\eta} & \text{otherwise} \end{cases} \tag{13}$$

with m=0.1 and η = 0.3.

In the following subsections, three variations of the SIMP approach are introduced, mainly by changing the filter used to regularize the sensitivity (for instance, using a distance filter computed via a convolution function and a Helmholtz-type filter) or by trying a time-advancing strategy (with multiple steps)

2.2 Theoretical Aspects of Vehicle Dynamics:

FSAE car was planned to use a double wishbone pushrod setup in front and rear suspension systems. Considering vehicle dynamics, weight distribution is set to 46% allocated to the front and 54% to the rear, with a total weight of 210 kg excluding the driver. Incorporating the driver's weight of 75 kg further refines the vehicle's load distribution and calculates dynamic behavior.

For Calculating Front Portion Weight

$$W_{front} = \left(W_{total\ car} \times \frac{46}{100}\right) = 131.1\ Kg$$

Here, the total car weight, including the driver, is 285 Kg, and the weight distribution is 46:54. So, each wheel has to carry 65.55 Kg.

For calculating spring travel, wheel travel, motion ratio, and ride frequency:

Spring travel = (Spring jounce + Spring rebound) = (35+16) = 51 mm

Wheel travel = (Wheel jounce + Wheel rebound) = (76.09+34.78) = 110.87 mm

Motion ratio, MR = $\frac{Spring\ Travel}{Wheel\ travel} = \frac{51}{110.87} = 0.46$

Ride frequency, f = $(\frac{1}{2\pi} \times \sqrt{\frac{K_S \times MR^2}{44.37}}) = 3.09$ Hz; Here, K_s = 78807 N/m, which is the spring stiffness of DNM RCP 2S.

The center of gravity height, established at 0.3 m, is a critical factor impacting the vehicle's stability and handling precision, especially during cornering and acceleration maneuvers. The wheel jounce travel, measured at 76.09 mm, denotes the maximum vertical displacement of the wheels during compression, while the corresponding rebound travel, at 34.78 mm, signifies the extension capacity. Similarly, the spring jounce and rebound travels, at 35 mm and 16 mm, respectively, highlight the corresponding displacement of the suspension springs, fundamental in modulating ride comfort and handling dynamics. The spring stiffness (K_s), quantified at 78807 N/m using the DNM RCP 2S spring, delineates the system's resistance to deflection under load, directly influencing its response to road irregularities. Additionally, the motion ratio of 0.46 was calculated. Ride frequency is a pivotal metric, as outlined by the FSAE Rulebook [33], with a recommended range of 2.5-3.5 Hz for optimal vehicle performance. Analysis reveals a calculated ride frequency of 6.7 Hz, exceeding the stipulated range. The spring stiffness (K_s) and ride frequency are at 16675.56 N/m and 3.09 Hz, respectively, aligning with regulatory guidelines and optimizing ride comfort and handling dynamics. Moreover, dynamic loading considerations are paramount, particularly during bump conditions where a force equivalent to 3 times the vehicle weight is applied to the suspension system. This translates to an individual force of (3 × 643.04) = 1929.14 N acting on each wheel during a bump event. Leveraging the geometric properties of the bell crank, precisely its triangular configuration, allows for the determination of the pushrod force (F_p) through trigonometric principles.

By employing trigonometry, the pushrod force, $F_p = \frac{1929.14}{\sin(90-\alpha)} = 2455.84$ N.

Concurrently, the total suspension force is derived as $F_s = (78807 \times \frac{35}{1000}) = 2758.25$ N.

Subsequently, the reaction force is computed utilizing vector analysis, yielding a value

$F_r = \sqrt{((2758.245)^2 + (1929.1)^2)} = 3365.93$ N.

Figure 1 presents the Free-Body Diagram (FBD) of the Formula Student (FSAE) bell crank, defining the essential boundary conditions and load cases required for the subsequent structural

topology optimization process.

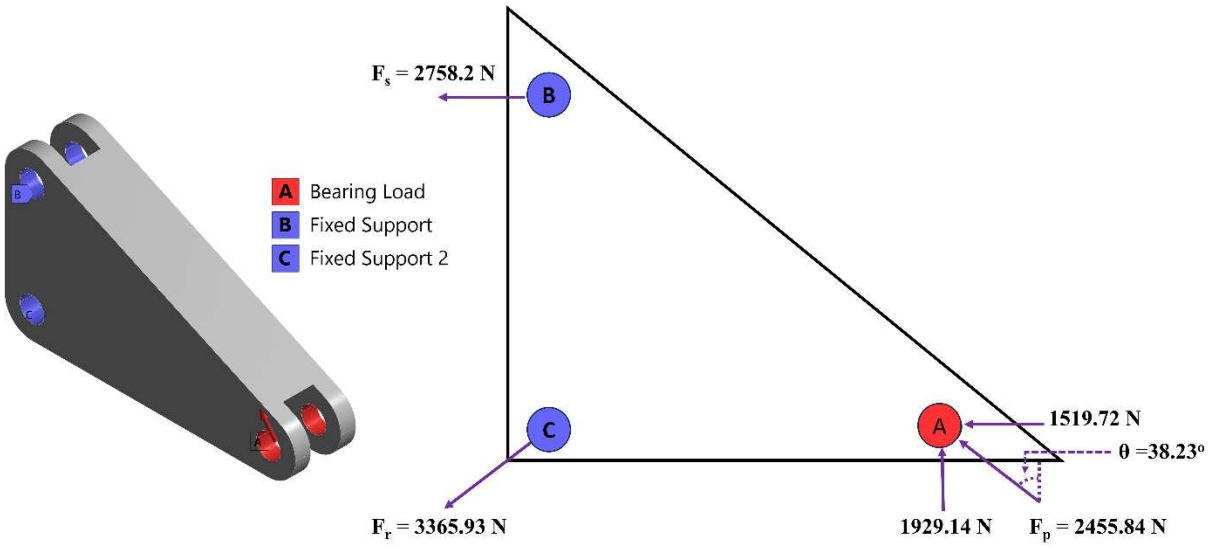


Figure 3: Bell crank's free body diagram

The design domain is constrained by two fixed supports at points B and C, which represent the chassis mounting locations, while point A serves as the bearing support where the actuation force is applied. The diagram illustrates a complex loading scenario where an input force F_p of 2455.84 N is applied at point A at an angle of 38.23°, resulting in horizontal and vertical components of 1519.72 N and 1929.14 N, respectively.

2.3 Selection of suitable material for the bell crank

Suspension components require long-lasting, strong, stiff, and inexpensive materials. Because suspension components are susceptible to dynamic loads, the material must also have a high fatigue strength. Considering these parameters, bell crank material must have a high Young's modulus, yield strength, fatigue strength, and low density. A weight-based comparative analysis was conducted on a specified set of materials. Every parameter (strength, density) received an equal weight of 100 points in this procedure. Weights are assigned based on the most desired value among the set of materials for a particular parameter and the value of the provided material. Table 1 displays the material and its accompanying parameter values for the comparison study, whereas Table 2 displays the results of the comparative study.

Table 1. Material properties and its cost

Materials	Yield Strength [Mpa]	Young Modulus [Mpa]	Density (Kg/m^{-3})
AISI 316L	518	193	8000
AISI 10 Mg	266	45	2680
Ti6Al4V	988	110	4420
In718	1088	120	8190
Aluminum 6063	145	68.9	2700
Aluminum 6061	276	68.9	2700
Mild Steel	250	200	7850
Stainless Steel	210	200	7930
Best	**1088**	**200**	**2680**
Worst	**145**	**45**	**8190**

Table 2. Results of Comparative study

Material	Yield Strength [Mpa]	Young Modulus [Mpa]	Density (Kg/m^{-3})	Total
AISI 316L	47.61	96.50	33.50	177.61
AISI 10 Mg	24.45	22.50	100.00	146.95
Ti6Al4V	**90.81**	**55.00**	**60.63**	**206.44**
In718	100.00	60.00	32.72	192.72
Aluminum 6063	13.33	34.45	99.26	147.04
Aluminum 6061	25.37	34.45	99.26	159.08
Mild Steel	22.98	100.00	34.14	157.12
Stainless Steel	19.30	100.00	33.80	153.10

As demonstrated in the scoring results, high-performance alloys such as Ti6Al4V (206.44 total points) and In718 (192.72 total points) achieved the highest scores due to their superior strength-

to-weight ratios, although Ti6Al4V ultimately emerged as the best material for its exceptional balance of structural integrity and lightweight properties. Conversely, while materials like AISI 316L and Aluminum 6061 offer better manufacturability and lower costs, their lower total scores reflect a trade-off in either excessive density or reduced yield strength compared to the specialized titanium and nickel-based superalloys.

2.4 Meshing

The Bell Crank mesh comprises 119,480 nodes and 78,441 elements with a 2 mm element size. The element order is set to "Program Control," the physics preference is configured for "Mechanical" to ensure accurate structural analysis. Figure-4 shows the mesh of the bell crack.

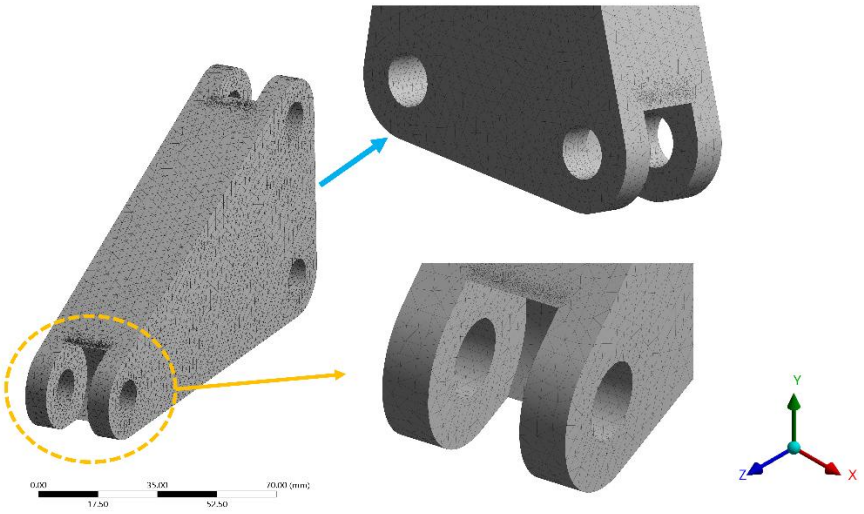


Figure-4: Mesh profile of Bell Crank of Formula Student Vehicle

3. Results and Discussion

A stress analysis was performed to compare various characteristics of the original and optimized bell cranks. In the FSAE Bell Crank analysis, equivalent stress was evaluated for each material under the same loading conditions. One of the most critical aspects in establishing the mechanical performance of a bell crank is Stress analysis. Here, eight types of material are analyzed,

comparing the equivalent Von Misses stress of the structure. In the base model, the equivalent stress varied from 58.6 MPa for AISI10 Mg to 61.4 MPa for AISI316L. Other materials, including structural steel, Ti 6414V, and mild steel, showed similar stresses of roughly 60.6 MPa.

Figure-5 illustrates the systematic material redistribution process used to optimize the FSAE bell crank for maximum structural efficiency. The sequence begins with (a), the initial design space representing the full volume mesh before optimization. As the iteration progresses through (b) and (c), finite element analysis (FEA) identifies and removes low-stress '**dead zones**.' The final stage, (d), showcases the optimized geometry, which achieves a 50% weight reduction while maintaining a high safety factor and ensuring that material is only present along critical load paths.

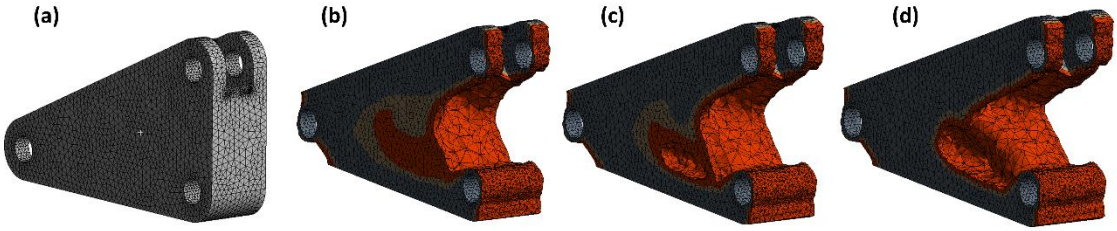


Figure-5: Topology optimization of bell crack

In the modified model, the stress across all materials was dropped to around 36.3 MPa. This indicates that topology optimization effectively reduced the stress on the bell crank. The stress values of the optimized materials were similar for all materials, with most converging around 36 MPa.

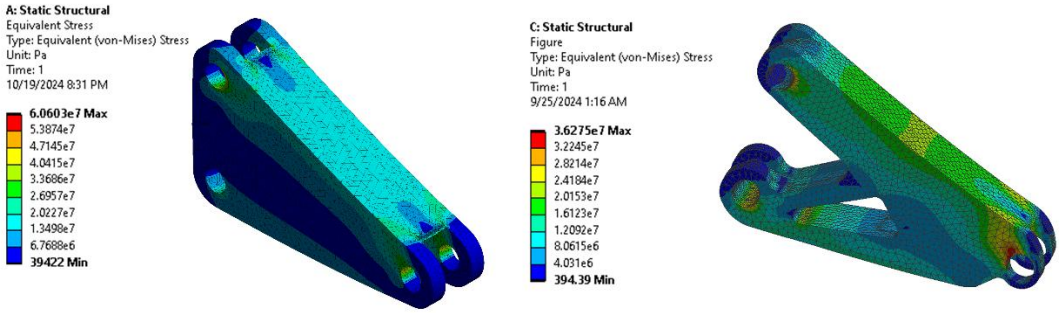


Figure-6: The Von Mises stress distribution of (a) Original Bell Crank, (b) Optimized bell crank

All materials showed considerable stress reductions after the topology optimization. The stress study reveals that topological optimization results in a significant reduction in equivalent stress for all materials. With corresponding increases in safety factors, the reductions vary from 38% to 41%. Ti 6414V, Inconel 718, and AISI316L are characterized by substantial safety factors and significant stress reductions, making them appropriate for high-stress settings. Aluminium alloys (6063 and 6061) have lower safety factors, suggesting they are more susceptible to high stress and, thus, less suitable for high-load applications than titanium alloys.

Total deformation demonstrates the flexibility and structural integrity of the material under load. Lower deformation values are preferable as they indicate higher stiffness and less structural flexing under loads. Fig shows the comparison of the deformation between the original model and the optimized model.

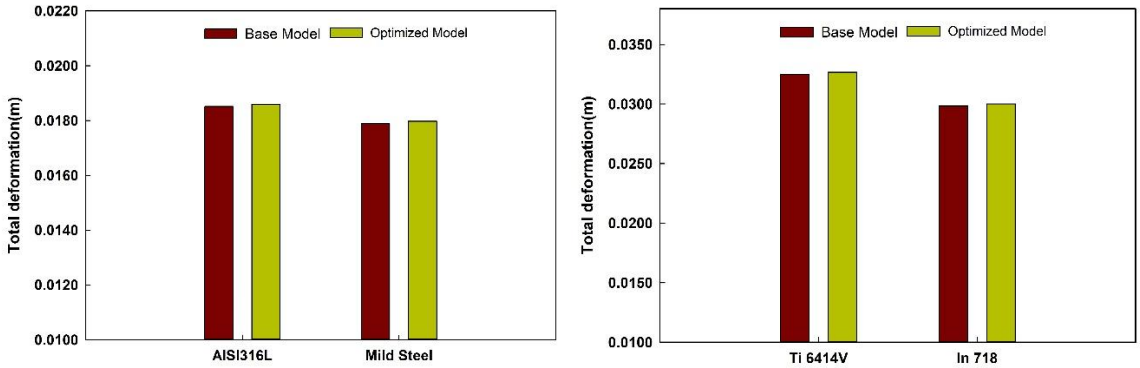


Figure-7: Comparison of Deformation in the Bell Crank Mild Steel, AISI 316L, Ti6Al4V and In718

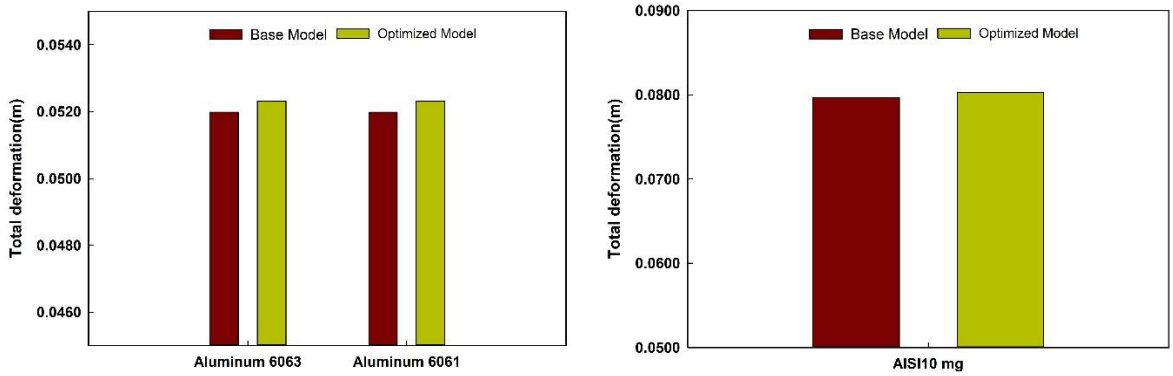


Figure-8: Comparison of Deformation in the Bell Crank AISI 10 Mg, Aluminum 6063, Aluminum 6061

The deformation remains almost unchanged for AISI316L. This indicates that it maintains excellent stiffness even after topology optimization. The base model exhibits significant

deformation at 0.079669 meters with the material AISI10 Mg, increasing slightly to 0.080256 meters. Even after mass reduction, the deformation remains high, indicating that AISI10 Mg may not be suitable for applications requiring high stiffness despite its low weight. Ti 6414V demonstrates moderate deformation of 0.032509 meters, which marginally increases to 0.032678 meters. It exhibits good stiffness and maintains its structural integrity even with mass reduction. Inconel 718 exhibits good rigidity, making it a viable option for reduced deformation. A notable mass reduction balances the slight increase in deformation. Aluminium 6063 and 6061 show significant deformation, making them less suitable for high-stiffness requirements. Minimal deformation is found with Mild Steel in both the base and optimized models. So, this can be a reliable material for applications demanding high structural rigidity while allowing for significant mass reduction.

The optimized models exhibit minimal deformation increases across all materials, implying that the topology optimization approach preserved the materials' structural integrity while lowering mass. Mild steel shows the least deformation in both basic and optimized models, making it the most rigid material. AISI316L and Ti 6414V maintain relatively low deformation and perform well, achieving significant mass reduction.

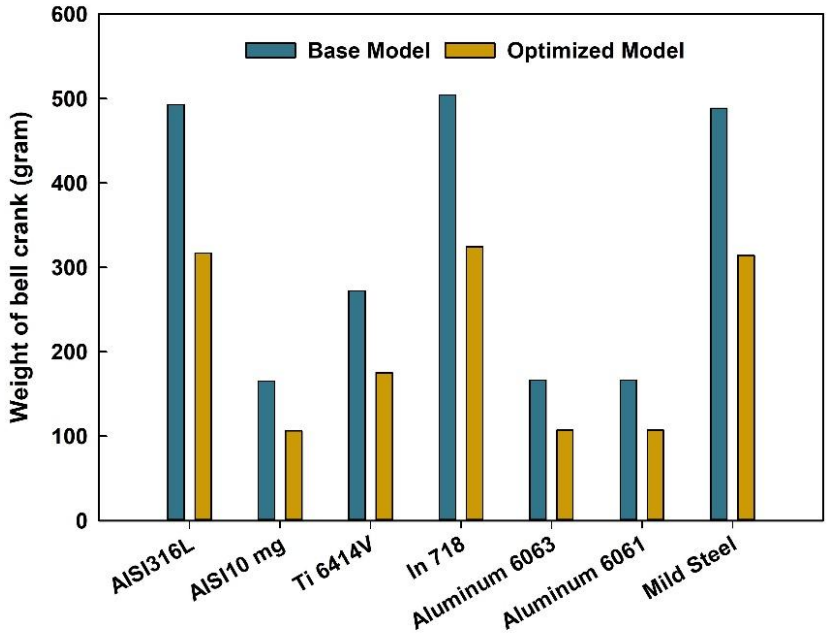


Figure-9: Comparison of initial and final weights of the bell crank

Across all materials, with 50% material removal the mass reduction achieved is 35.68% post-optimization. The increase in the safety factor ranges from 64% to 82%, depending on the material. Materials like Ti 6414V, Inconel 718, and AISI316L show excellent weight reduction while maintaining high safety margins, making them ideal for applications with both lightweight and high-strength performance.

4. Conclusion

This work focused on optimizing the topology of the FSAE Bell Crank with various materials to reduce weight, increase safety factor, and reduce deformation under load. The computational study of the bell crank was conducted in ANSYS and then examined for stress distribution. Based on the stress distribution, the areas with low stress were removed to reduce the weight. The removed zones were then finished to make the material removal manufacturing-friendly. Based on the results from the stress, deformation, and mass reduction analyses, the conclusions of this study are:

- Titanium alloy (Ti 6414V) emerged as the best material, with a high safety factor (15.0), significant stress reduction (40%), and low deformation. It provides an excellent balance of lightweight, strength, and structural integrity. However, Ti 6414V is more difficult to manufacture due to its high cost and machining complexity, resulting in longer lead times and higher overall production costs. Inconel 718 also performed well, but it is also expensive and difficult to machine, making it less practical for large-scale manufacturing.
- AISI316L shows its rigidity for use in moderately loaded components, with a substantial increase in the safety factor (from 8.43 to 14.28) and stress reduction. It is also widely available, easy to machine, and more cost-effective than titanium or Inconel, making it a practical choice for mass production.
- Shape optimization reduces the weight of machine components while maintaining their strength. In this study, the component's ultimate weight was lowered by 25-30% from its beginning weight.
- Weight reduction can help reduce automobile material usage and fuel consumption.

Declaration

Acknowledgments

The authors warmly credit the simulation lab for providing the computer resources.

Funding

The authors affirm that they did not accept any outside funds, grants, or other kinds of assistance to write this paper.

Author Contributions

The original concept and layout of the modeling were contributions from all creators. The final manuscript was reviewed and approved by all writers.

Khairun Nasrin Rimi worked for conceptualization, simulation and supervision. Md saifur Rahman did data curation and Original draft preparation. Md Araful Haque did visualization, investigation and formatting. Nurul Islam Kajol, Zannatul Ferdous worked for Writing- Reviewing and Editing.

Availability of data and materials

The datasets found and analyzed during the current study are available in this paper.

Competing interests

The authors declare that they have no competing interests.

Clinical Trial Registration

Not applicable

Clinical trial number

Not applicable.

Ethics and Consent to Participate

Not applicable

Consent for Publication

Not applicable

References

[1] SAE International (2026) Advancing mobility knowledge and solutions: Formula SAE rules. https://www.sae.org/attend/student-events/formula-sae/rules. Accessed 12 Jan 2026

[2] Saurabh YS et al (2016) Design of suspension system for Formula Student race car. Procedia Eng 144:1138–1149. doi:10.1016/j.proeng.2016.05.081

[3] SAE International (2026) Fundamentals of Vehicle Suspension design. https://www.sae.org/learn/content/c1618. Accessed 12 Jan 2026

[4] Vadhe AA (2018) Design and Optimization of Formula SAE Suspension system. Int J Curr Eng Technol 8(3). doi:10.14741/ijcet/v.8.3.17

[5] Pang TY, Fard M (2020) Reverse engineering and topology optimization for Weight-Reduction of a Bell-Crank. Appl Sci 10(23):8568. doi:10.3390/app10238568

[6] Organ AJ (2007) 'How to make a business out of Stirling engines today'. In: Elsevier eBooks, pp 226–251. doi:10.1533/9781845693602.4.226

[7] Aulig N, Nutwell E, Menzel S et al (2017) Preference-based topology optimization for vehicle concept design with concurrent static and crash load cases. Struct Multidiscip Optim 57(1):251–266. doi:10.1007/s00158-017-1751-z

[8] Bendsøe MP, Sigmund O (2004) Topology Optimization. Springer. doi:10.1007/978-3-662-05086-6

[9] Tsavdaridis KD, Efthymiou E, Adugu A et al (2019) Application of structural topology optimisation in aluminium cross-sectional design. Thin-Walled Struct 139:372–388. doi:10.1016/j.tws.2019.02.038

[10] Wu J, Sigmund O, Groen JP (2021) Topology optimization of multi-scale structures: a review. Struct Multidiscip Optim 63(3):1455–1480. doi:10.1007/s00158-021-02881-8

[11] Sigmund O, Maute K (2013) Topology optimization approaches. Struct Multidiscip Optim 48(6):1031–1055. doi:10.1007/s00158-013-0978-6

[12] Jankovics D, Barari A (2019) Customization of Automotive Structural Components using Additive Manufacturing and Topology Optimization. IFAC-PapersOnLine 52(10):212–217. doi:10.1016/j.ifacol.2019.10.066

[13] Lim J, You C, Dayyani I (2020) Multi-objective topology optimization and structural analysis of periodic spaceframe structures. Mater Des 190:108552. doi:10.1016/j.matdes.2020.108552

[14] Zhong Y et al (2023) Visualization analysis of research hotspots on structural topology optimization based on CiteSpace. Sci Rep 13(1):18166. doi:10.1038/s41598-023-45447-y

[15] Bendsøe MP, Sigmund O (1999) Material interpolation schemes in topology optimization. Arch Appl Mech 69(9–10):635–654. doi:10.1007/s004190050248

[16] Zhang S, Li H, Huang Y (2020) An improved multi-objective topology optimization model based on SIMP method for continuum structures including self-weight. Struct Multidiscip Optim 63(1):211–230. doi:10.1007/s00158-020-02685-2

[17] Xia M, Zhou Q, Sykulski J et al (2020) A Multi-Objective Topology Optimization methodology based on Pareto Optimal Min-Cut. IEEE Trans Magn 56(3):1–5. doi:10.1109/tmag.2019.2955386

[18] Mesicek J, Pagac M, Petru J et al (2019) TOPOLOGICAL OPTIMIZATION OF THE FORMULA STUDENT BELL CRANK. MM Sci J 2019(03):2964–2968. doi:10.17973/mmsj.2019_10_201893

[19] Fornace LV, Benson D, Murakami H (2006) Weight Reduction Techniques Applied to Formula SAE Vehicle Design: An investigation in Topology Optimization. University of California, San Diego

[20] Divadkar S, Dhatrak P (2023) Topology Optimization of a Bell Crank Lever Based on Stiffness and Mass using Finite Element Analysis. E3S Web Conf 430:01266. doi:10.1051/e3sconf/202343001266

[21] Chauhan P, Sah K, Kaushal R (2020) Design, modeling and simulation of suspension geometry for formula student vehicles. Mater Today Proc 43:17–27. doi:10.1016/j.matpr.2020.11.200

[22] Nandanwar T, Waghela K, Gupta E et al (2021) TOPOLOGY OPTIMIZATION OF THE BELL CRANK & BRAKE PEDAL. IOP Conf Ser Mater Sci Eng 1123(1):012035. doi:10.1088/1757-899x/1123/1/012035

[23] Chang JW, Lee YS (2008) Topology optimization of compressor bracket. J Mech Sci Technol 22(9):1668–1676. doi:10.1007/s12206-008-0428-3

[24] Wu P, Ma Q, Luo Y et al (2016) Topology Optimization design of automotive engine bracket. Energy Power Eng 8(04):230–235. doi:10.4236/epe.2016.84021

[25] Sudin MN, Tahir M, Ramli F et al (2014) Topology Optimization in Automotive Brake pedal Redesign. J Adv Rev Sci Res 1(1):1–11

[26] Zhang E, Wang L (2020) Finite element analysis and topology optimization design of seat bracket for new energy bus. J Phys Conf Ser 1550(4):042038. doi:10.1088/1742-6596/1550/4/042038

[27] Zhu J-H, Zhang W-H, Xia L (2015) Topology optimization in aircraft and aerospace structures design. Arch Comput Methods Eng 23(4):595–622. doi:10.1007/s11831-015-9151-2

[28] Xiao Q, Guo W-N, Yang L-T et al (2020) Design and topology optimization of air conditioning suspension bracket for metro. Sci Prog 103(4). doi:10.1177/0036850420980617

[29] Guo X, Zhang W, Zhang L (2012) Robust structural topology optimization considering boundary uncertainties. Comput Methods Appl Mech Eng 253:356–368. doi:10.1016/j.cma.2012.09.005

[30] Park J, Lee D, Sutradhar A (2019) Topology optimization of fixed complete denture framework. Int J Numer Method Biomed Eng 35(6):e3193. doi:10.1002/cnm.3193

[31] Koper DC, Leung CAW, Smeets LCP et al (2020) Topology optimization of a mandibular reconstruction plate and biomechanical validation. J Mech Behav Biomed Mater 113:104157. doi:10.1016/j.jmbbm.2020.104157

[32] Yago D, Cante J, Lloberas-Valls O et al (2021) Topology Optimization Methods for 3D Structural Problems: A Comparative study. Arch Comput Methods Eng 29(3):1525–1567. doi:10.1007/s11831-021-09626-2

[33] SAE International (2026) Formula SAE. https://www.fsaeonline.com/cdsweb/gen/documentresources.aspx. Accessed 12 Jan 2026